Article

Cell Reports

Epithelial HMGB1 Delays Skin Wound Healing and Drives Tumor Initiation by Priming Neutrophils for NET Formation

Graphical Abstract

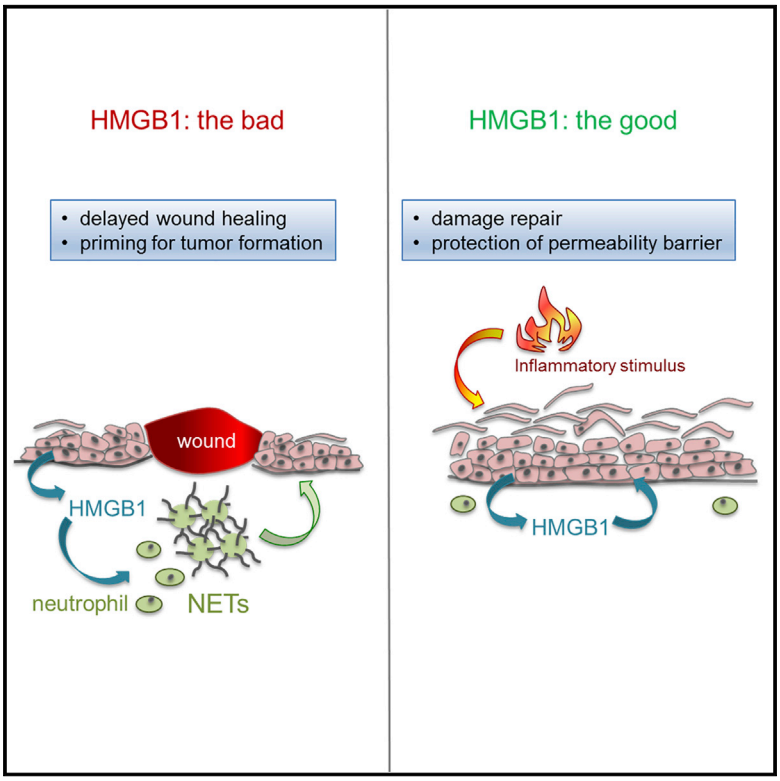

Authors

Esther Hoste, Christian Maueröder, Lisette van Hove, ..., Yvan Saeys, Robert Felix Schwabe, Geert van Loo

Correspondence

esther.hoste@irc.vib-ugent.be (E.H.), geert.vanloo@irc.vib-ugent.be (G.v.L.)

In Brief

Inflammation mediates tissue repair but can be hijacked to promote tumorigenesis. Hoste et al. demonstrate that HMGB1 delays regeneration and drives tumor formation in skin by recruitment and priming of neutrophils. These data indicate that therapies targeting HMGB1 or NET formation might be relevant in chronic and diabetic wound treatment.

Highlights

- HMGB1 controls transition from pre-cancerous to cancerous lesions in skin
- Epithelial HMGB1 promotes neutrophil recruitment and NET formation
- TNF and RIPK1 activity mediate HMGB1-dependent NET formation and skin tumorigenesis
- NET formation occurs in lesional and tumor-associated skin of RDEB patients

Hoste et al., 2019, Cell Reports *29*, 2689–2701
November 26, 2019
https://doi.org/10.1016/j.celrep.2019.10.104

CellPress

Cell Reports
Article

Epithelial HMGB1 Delays Skin Wound Healing and Drives Tumor Initiation by Priming Neutrophils for NET Formation

Esther Hoste,[1,2,14,*] Christian Maueröder,[1,2] Lisette van Hove,[1,2] Leen Catrysse,[1,2] Hanna-Kaisa Vikkula,[1,2] Mozes Sze,[1,2] Bastiaan Maes,[1] Dyah Karjosukarso,[3] Liesbet Martens,[1,2] Amanda Gonçalves,[1,2,4] Eef Parthoens,[1,2,4] Ria Roelandt,[1,2] Wim Declercq,[1,2] Ignacia Fuentes,[5,6] Francis Palisson,[5,7] Sergio Gonzalez,[8] Julio C. Salas-Alanis,[9] Louis Boon,[10] Peter Huebener,[11] Klaas Willem Mulder,[3] Kodi Ravichandran,[1,2] Yvan Saeys,[1,13] Robert Felix Schwabe,[12] and Geert van Loo[1,2,*]

[1]VIB Center for Inflammation Research, 9052 Ghent, Belgium
[2]Department of Biomedical Molecular Biology, Ghent University, 9052 Ghent, Belgium
[3]Department of Molecular Developmental Biology, Radboud University, 6525 XZ Nijmegen, the Netherlands
[4]VIB Bio-Imaging Core, 9052 Ghent, Belgium
[5]Fundación DEBRA Chile, Santiago, Chile
[6]Centro de Genetica y Genomica, Clinica Allemana, Universidad de Desarrollo, Santiago, Chile
[7]Facultad de Medicina, Universidad de Desarrollo, Santiago, Chile
[8]Departemento de Patología, Facultad de Medicina, Pontificia Universidad Católica de Chile, Santiago, Chile
[9]DEBRA Mexico, Monterrey N.L., Mexico
[10]Bioceros, 3584 CM Utrecht, the Netherlands
[11]Department of Internal Medicine, University Medical Center Hamburg-Eppendorf, 20246 Hamburg, Germany
[12]Department of Medicine, Columbia University, New York, NY 10019, USA
[13]Department of Applied Mathematics, Computer Sciences and Statistics, Ghent University, 9052 Ghent, Belgium
[14]Lead Contact
*Correspondence: esther.hoste@irc.vib-ugent.be (E.H.), geert.vanloo@irc.vib-ugent.be (G.v.L.)
https://doi.org/10.1016/j.celrep.2019.10.104

SUMMARY

Regenerative responses predispose tissues to tumor formation by largely unknown mechanisms. High-mobility group box 1 (HMGB1) is a danger-associated molecular pattern contributing to inflammatory pathologies. We show that HMGB1 derived from keratinocytes, but not myeloid cells, delays cutaneous wound healing and drives tumor formation. In wounds of mice lacking HMGB1 selectively in keratinocytes, a marked reduction in neutrophil extracellular trap (NET) formation is observed. Pharmacological targeting of HMGB1 or NETs prevents skin tumorigenesis and accelerates wound regeneration. HMGB1-dependent NET formation and skin tumorigenesis is orchestrated by tumor necrosis factor (TNF) and requires RIPK1 kinase activity. NETs are present in the microenvironment of keratinocyte-derived tumors in mice and lesional and tumor skin of patients suffering from recessive dystrophic epidermolysis bullosa, a disease in which skin blistering predisposes to tumorigenesis. We conclude that tumorigenicity of the wound microenvironment depends on epithelial-derived HMGB1 regulating NET formation, thereby establishing a mechanism linking reparative inflammation to tumor initiation.

INTRODUCTION

Danger-associated molecular patterns (DAMPs) activate the immune system upon injury and have key roles in cancer by either promoting inflammation or by driving the cytotoxic anti-tumor host response (Hernandez et al., 2016). However, the specific contribution of individual DAMPs in these processes are still enigmatic. High-mobility group box 1 (HMGB1) is a multifunctional protein that serves as a transcriptional regulator in the nucleus but upon secretion acts as a DAMP, potently activating inflammation (Scaffidi et al., 2002). HMGB1 performs its cytokine function by binding to various receptors, the best documented being RAGE (receptor for advanced glycation end products) and TLR-4 (Toll-like receptor 4) (Hori et al., 1995; Yang et al., 2010). Increased levels of circulating HMGB1 have been shown to amplify the inflammatory responses that regulate tumor progression, invasion, and metastasis (Kang et al., 2013), but the importance of HMGB1 in initiating neoplastic responses is largely unknown. In skin, we previously showed that flagellated bacteria can trigger TLR-5 activation in leukocytes, inducing the upregulation of cutaneous HMGB1 expression levels and the promotion of wound-induced tumorigenesis (Hoste et al., 2015). Although HMGB1 has previously been implicated in tissue regeneration (Huebener et al., 2015; Straino et al., 2008; Tirone et al., 2018), the molecular mechanisms through which this DAMP mediates wound repair and neoplastic events in skin are still unknown.

Chronic and acute wounding predisposes tissues to tumor formation (Arwert et al., 2012). In skin, this association is remarkably

clear in patients suffering from recessive dystrophic epidermolysis bullosa (RDEB), a rare genetic cutaneous blistering disorder. Skin of RDEB patients constantly undergoes injury and repair, predisposing the epidermis to squamous cell carcinoma (SCC) formation (Fine et al., 2009). We previously demonstrated that HMGB1 is abundantly secreted in SCC-associated skin of RDEB patients (Hoste et al., 2015). Moreover, levels of circulating HMGB1 have been shown to correlate with RDEB disease severity (Petrof et al., 2013). Neutrophils are the first immune cells recruited to wounded skin, where they can form neutrophil extracellular traps (NETs), enabling neutrophils to fight pathogens (Belaaouaj et al., 1998; Brinkmann et al., 2004). NET formation is characterized by the release of neutrophil chromatin decorated with antimicrobial peptides in order to trap and potentially kill pathogens. Although being an important antimicrobial defense mechanism, NETs can also induce tissue damage, as is the case in diabetic conditions, where neutrophils are primed to form NETs, thereby delaying cutaneous wound healing (Menegazzo et al., 2015; Wong et al., 2015). Since NETs have also been shown to impact on a plethora of diseases, including asthma and arthritis (Jorch and Kubes, 2017; Khandpur et al., 2013; Toussaint et al., 2017), and have been observed in the microenvironment of various tumor types (Demers et al., 2016), inhibiting NET formation might be an interesting therapeutic strategy to treat disease. One important cytokine that has been implicated in neutrophil priming is tumor necrosis factor (TNF) (Yuo et al., 1991), which is also important for chemical- and wound-induced skin carcinogenesis (Hoste et al., 2015; Moore et al., 1999), implicating a role for TNF in mediating NET formation downstream of HMGB1 release.

Here, we tested the hypothesis that a sole DAMP, namely HMGB1, impacts on pathological cutaneous remodeling and tumor initiation. We could demonstrate a crucial role for epithelial-derived HMGB1 in regenerative and neoplastic inflammation and show that keratinocyte-specific HMGB1 primes neutrophils for NET formation in full-thickness skin wounds, resulting in delayed cutaneous wound closure and pro-tumorigenic signaling via TNF and RIPK1 kinase signaling. These findings identify epithelial-derived HMGB1 as a crucial molecule mediating tumorigenicity of the wound microenvironment and suggest that HMGB1 neutralization or inhibition of NET formation may have potential as a therapeutic strategy to prevent skin cancer and accelerate cutaneous wound healing responses.

RESULTS

Keratinocyte-Specific HMGB1 Delays Wound Healing and Promotes Skin Tumor Formation

In order to understand the *in vivo* function of HMGB1 as a DAMP in cutaneous regenerative and neoplastic responses, we selectively deleted HMGB1 in keratinocytes or monocytes/macrophages by crossing HMGB1 "floxed" mice (Huebener et al., 2015) to mice expressing keratin-5 Cre (Tarutani et al., 1997) or lysozyme M Cre (Clausen et al., 1999), respectively (Figures S1A and S1B). Neither keratinocyte-specific HMGB1 knockout (Δ^{Ker} HMGB1) mice nor myeloid-specific HMGB1 knockout (Δ^{myelo} HMGB1) mice displayed overt phenotypes. However, when subjected to full-thickness skin wounding, healing rates were markedly accelerated in Δ^{Ker} HMGB1 mice relative to littermate $HMGB1^{fl/fl}$ (Cre negative) control mice (Figure 1A; Figure S1C). Interestingly, wound healing rates were indistinguishable between mice lacking HMGB1 in myeloid cells and control littermates (Figure S1D). The accelerated wound healing rates observed in Δ^{Ker} HMGB1 skin were not due to cell-autonomous keratinocyte effects, as primary keratinocytes in culture showed faster healing effects in scratch-wound assays in HMGB1-proficient versus HMGB1-deficient cultures (Figure S1E). HMGB1 is upregulated in various chronically inflamed conditions (Degryse et al., 2001; Taniguchi et al., 2003); therefore, we next investigated wound healing responses in transgenic mice expressing a constitutively active MAP-kinase kinase 1 (MEK1) in differentiating keratinocytes (InvEE mice). These mice exhibit chronic skin inflammation, allowing the study of wound healing responses in a pathological skin context (Hobbs et al., 2004). Upon skin wounding, InvEE mice lacking HMGB1 in keratinocytes closed their wounds markedly faster than HMGB1-proficient InvEE mice (Figure 1B; Figure S1F). In contrast, myeloid-cell-specific deletion of HMGB1 in InvEE mice did not result in altered wound closure rates (Figure S1G). Together, these data indicate that HMGB1 derived from keratinocytes, but not myeloid cells, plays an important role in reparative cutaneous inflammation.

HMGB1 has a context-dependent role in either promoting tumorigenesis by triggering chronic inflammation or in protecting from tumor development by eliciting immunogenic cell death (Hernandez et al., 2016; Kang et al., 2013). To unravel the function of HMGB1 in cutaneous tumor initiation, we subjected InvEE mice lacking HMGB1 in either keratinocytes or in myeloid cells to wound-induced tumor formation. InvEE mice develop tumors at sites of full-thickness skin wounding with an incidence of 50% (Arwert et al., 2010). Strikingly, Δ^{Ker} HMGB1 mice were completely protected from wound-induced tumor formation (Figure 1C), while Δ^{myelo} HMGB1 mice were equally sensitive to InvEE papillomagenesis (Figure S1H). Given that HMGB1 has important roles in the nucleus where it mediates the assembly of transcription factor complexes (Park et al., 2003; West et al., 2004), we tested wound healing rates and skin tumorigenesis in the presence of Box A, an HMGB1 antagonist that prevents HMGB1 binding to its receptors (Kokkola et al., 2003). In agreement with the faster wound healing rates observed in Δ^{Ker} HMGB1 mice (Figure 1B), accelerated wound closure was also observed in InvEE mice that were intradermally injected with Box A at time of wounding and during early stages of repair (Figure 1D), and subsequent wound-induced tumor formation was strongly reduced upon Box A treatment (Figure 1E). Additionally, we intradermally injected mice with ethylpyruvate, an established inhibitor of HMGB1 secretion (Davé et al., 2009; Kim et al., 2016), and also observed a protective effect on InvEE papillomagenesis (Figure 1F). In order to identify the receptor through which HMGB1 mediates regenerative and tumorigenic responses in skin, we next injected InvEE mice with antagonistic agents against RAGE or TLR-4. Both TLR-4 as well as RAGE neutralization resulted in enhanced wound closure in early post-wounding stages (Figures S1I and S1J). In addition, treatment with a monoclonal TLR-4 blocking antibody at the time of wounding and during the early post-wounding stages

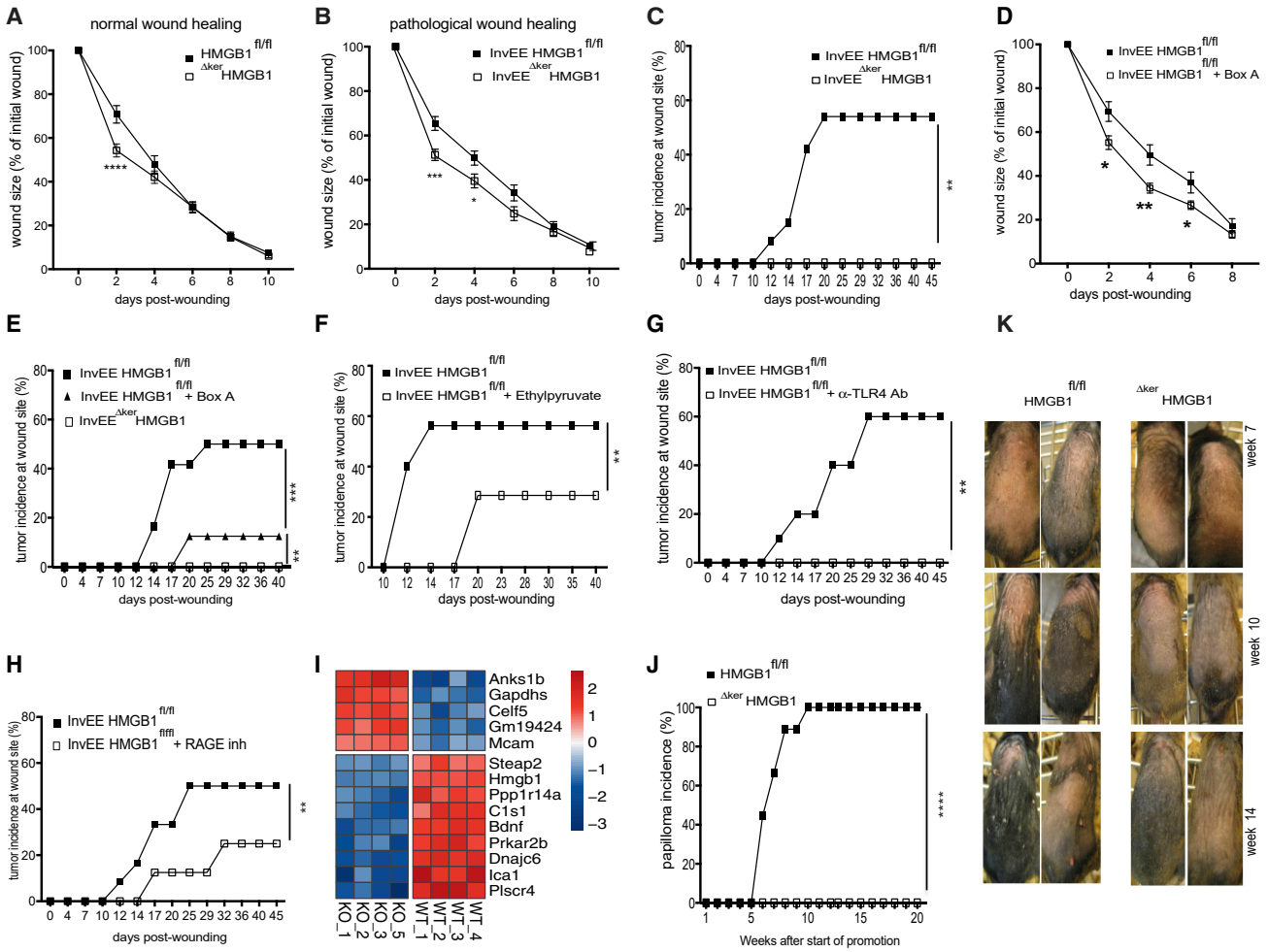

Figure 1. Keratinocyte-Specific HMGB1 Delays Wound Healing and Promotes Skin Tumor Formation

(A and B) Wound healing dynamics of wild-type (HMGB1$^{fl/fl}$, n = 17) and Δ^{Ker} HMGB1 (n = 14) mice (A) or InvEE HMGB1$^{fl/fl}$ (n = 24) and InvEE Δ^{Ker} HMGB1 (n = 15) mice (B) after full-thickness wounding with an 8 mm punch biopsy (*p < 0.05; ***p < 0.001; ****p < 0.0001 between groups on respective days post-wounding; two-way ANOVA with multiple comparisons).

(C) Incidence of papilloma formation in InvEE HMGB1$^{fl/fl}$ (n = 26) and InvEE Δ^{Ker} HMGB1 (n = 17) mice at site of wounding (**p = 0.002; Wilcoxon matched-pairs signed rank test).

(D and E) Wound healing dynamics (D) and wound-induced tumor incidence (E) in InvEE HMGB1$^{fl/fl}$ (n = 12) and InvEE Δ^{Ker} HMGB1 (n = 12) mice intradermally injected with PBS (vehicle) or with Box A (n = 8) at time of wounding and 12, 24, and 36 h post-wounding (**p = 0.0016; *p < 0.05; two-way ANOVA with multiple comparisons).

(F) Wound-induced tumor incidence in InvEE HMGB1$^{fl/fl}$ mice intradermally injected with PBS (n = 16) or with ethylpyruvate (n = 7) at time of wounding and 12, 24, and 36 h post-wounding (**p = 0.0039; Wilcoxon matched-pairs signed rank test).

(G) Wound-induced tumor incidence in InvEE HMGB1$^{fl/fl}$ mice intradermally injected with IgG (n = 10) or with a monoclonal TLR-4-inhibiting antibody (n = 10) at time of wounding and 12, 24, and 36 h post-wounding (**p = 0.002; Wilcoxon matched-pairs signed rank test).

(H) Wound-induced tumor incidence in InvEE HMGB1$^{fl/fl}$ mice intradermally injected with PBS (n = 12) or with a RAGE antagonistic peptide (n = 8) at time of wounding and 12, 24, and 36 h post-wounding (**p = 0.002; Wilcoxon matched-pairs signed rank test).

(I) Heatmap depicting mean expression of differentially expressed genes between InvEE HMGB1$^{fl/fl}$ and InvEE Δ^{Ker} HMGB1 keratinocytes.

(J) Incidence of papilloma formation in HMGB1$^{fl/fl}$ (n = 26) and Δ^{Ker} HMGB1 (n = 17) mice treated with DMBA and TPA (****p < 0.0001; Wilcoxon matched-pairs signed rank test).

(K) Representative photographs of HMGB1$^{fl/fl}$ and Δ^{Ker} HMGB1 mice treated with DMBA and TPA at week 7, 10, and 14 after start of TPA treatment. Wound healing data represent mean ± SEM.

See also Figure S1.

completely protected InvEE mice from tumor development (Figure 1G). Treatment with a blocking peptide against RAGE also protected InvEE mice from wound-induced tumorigenesis, albeit to a lesser extent than treatment with a TLR-4 inhibiting antibody (Figure 1H). RNA sequencing of sorted live integrin-alpha 6-positive keratinocytes obtained from InvEE Δ^{Ker} HMGB1 and InvEE

HMGB1-proficient mice indicated that HMGB1 is the sole cytokine that is differentially expressed in both genotypes (Figure 1I; Figure S1K; GEO: GSE138918).

In order to confirm our observations in the InvEE model of wound-induced tumorigenesis in an independent skin tumor model, we next subjected Δ^{Ker} HMGB1 and control littermates to the two-stage chemically induced DMBA/TPA (7,12-dimethylbenz(a)anthracene and 12-O-tetradecanoylphorbol-13-acetate) skin carcinogenesis model. In this model, skin cancer is induced by exposure to a single dose of DMBA inducing oncogenic mutations in HRas (initiation), followed by the repeated topical application with the phorbol ester TPA (promotion) allowing mutagenized cells to expand and form benign papillomas (Abel et al., 2009). In agreement with the phenotype observed in wound-induced tumorigenesis, mice lacking HMGB1 in keratinocytes were also fully resistant to chemically induced tumor formation (Figures 1J and 1K). Together, these data prove that keratinocyte-derived HMGB1 is a key DAMP that delays regenerative wound healing responses and initiates neoplasia in chronically inflamed skin.

Keratinocyte-Specific HMGB1-Deficient Mice Exhibit an Exacerbated Cutaneous Response to TPA Treatment

HMGB1, in its function as a DAMP, has been characterized as a potent pro-inflammatory mediator (Scaffidi et al., 2002; Wang et al., 1999). To investigate whether the complete resistance of Δ^{Ker} HMGB1 mice to chemically induced skin tumor formation was due to reduced inflammation upon treatment with the pro-inflammatory phorbol ester TPA, we examined the response of Δ^{Ker} HMGB1 skin to topical TPA treatment. For this, Δ^{Ker} HMGB1 and control littermate mice were repetitively treated with TPA for a total of two to six applications, and skin was collected 24 h after the last treatment (Figure 2A). Surprisingly, Δ^{Ker} HMGB1 mice exhibited an exacerbated response to TPA relative to HMGB1$^{fl/fl}$ control mice. After two topical TPA treatments, a significantly higher increase in transepidermal water loss (TEWL) was observed in Δ^{Ker} HMGB1 compared to control mice. This response was even more pronounced in skin of Δ^{Ker} HMGB1 mice treated six times with TPA (Figure 2B), indicating a more severe skin barrier perturbation in the absence of keratinocyte-derived HMGB1. In agreement, an increase in epidermal thickness could be observed in skin of TPA-treated Δ^{Ker} HMGB1 mice relative to HMGB1$^{fl/fl}$ skin (Figures 2C and 2D), again indicating a more severe tissue response to the pro-inflammatory exposure to TPA in Δ^{Ker} HMGB1 skin relative to control skin.

To further discriminate between the effect of HMGB1 deficiency in keratinocytes on DMBA-induced tumor formation versus TPA-mediated tumor promotion, we subjected Δ^{Ker} HMGB1 mice and control littermates to topical DMBA treatment twice a week for 15 weeks. Δ^{Ker} HMGB1 mice were able to mount a tumor-protective response to treatment with the carcinogen alone, as tumor formation was strongly delayed upon DMBA treatment (Figure 2E). However, in contrast to the DMBA/TPA model, to which Δ^{Ker} HMGB1 mice were fully resistant, tumors did arise in Δ^{Ker} HMGB1 mice treated with DMBA alone, albeit far later and to fewer extent than in control littermates (Figure 2E; Figure S2). In conclusion, given that Δ^{Ker} HMGB1 mice exhibit an enhanced sensitivity to epidermal barrier perturbation upon repetitive treatment with the phorbol ester TPA relative to their HMGB1$^{fl/fl}$ littermates, the tumor-protective effect of HMGB1 ablation in keratinocytes does not result from a reduced inflammatory response in these mice. However, our data indicate that, depending on the type of epithelial damage, keratinocyte-derived HMGB1 can either protect from epidermal barrier perturbation or delay epithelial repair.

Epithelial-Derived HMGB1 Mediates Neutrophil Infiltration and NET Formation in Skin Wounds

Neutrophils represent the first immune cell type that is recruited to sites of injury. Interestingly, genes encoding for proteins involved in neutrophil infiltration, such as the chemokines *Cxcl-2* and *Ccl5* (*RANTES*), were significantly downregulated in TPA-treated Δ^{Ker} HMGB1 mice relative to controls (Figure 3A). These findings are in agreement with the reduced neutrophil infiltration seen in livers of acetaminophen-intoxicated hepatocyte-specific HMGB1-deficient mice (Huebener et al., 2015). Therefore, we tested whether neutrophil infiltration is altered in wounds of mice lacking HMGB1 in keratinocytes. Indeed, as shown by flow cytometric analysis, the total amount of neutrophils (CD45+ CD11b+ Ly6-G+ cells) that infiltrated the skin at day 2 post-wounding was significantly lower in Δ^{Ker} HMGB1 compared to HMGB1$^{fl/fl}$ mice. In contrast, the total amount of macrophages (CD45+ CD11b+ CD64+ cells) present in these wounds did not differ between genotypes (Figures 3B and 3C).

Neutrophils can form extracellular traps, termed NETs, which have been demonstrated to delay cutaneous wound healing responses (Wong et al., 2015). Given that we observed slower wound closure in HMGB1$^{fl/fl}$ relative to Δ^{Ker} HMGB1 mice, we analyzed whether the level of NET formation was reduced in Δ^{Ker} HMGB1 wounds. Western blot analysis of skin wound lysates showed prominent levels of citrullinated histone-3 (H3^{citr}), an established marker for NET formation (Wong et al., 2015; Toussaint et al., 2017), in HMGB1-proficient wounds, whereas H3^{citr} levels are barely detectable in Δ^{Ker} HMGB1 wounds at day 2 post-wounding (Figure 3D). NETs are defined as neutrophilic extracellular DNA structures that colocalize with granule-derived proteins and histones (Konig and Andrade, 2016; Boeltz et al., 2019). We performed immunofluorescent staining of externalized DNA (DAPI) and assessed colocalization with neutrophil elastase (NE) and H3^{citr}. Confocal microscopy of skin wounds of Δ^{Ker} HMGB1 and HMGB1$^{fl/fl}$ mice at early post-wounding stage verified that NET formation was markedly reduced in Δ^{Ker} HMGB1 wounds relative to control littermates (Figure 3E). NETs were also observed in the tumor stroma of wound-induced papillomas (Figure 3E) but were absent in unwounded Δ^{Ker} HMGB1 and HMGB1$^{fl/fl}$ mice. We also confirmed the reduced level of histone-3 citrullination in neutrophils in Δ^{Ker} HMGB1 skin wounds by flow cytometric quantification of live neutrophils (CD45+ CD11b+ Ly6G+ cells) that stained for citrullinated histone-3 in Δ^{Ker} HMGB1 and HMGB1$^{fl/fl}$ wounds at day 2 post-wounding (Figure 3F), although it should be stated that this might be due to the reduced neutrophil infiltration observed in Δ^{Ker} HMGB1 wounds. In conclusion, we could demonstrate that keratinocyte-derived HMGB1 drives neutrophil infiltration and NET formation in the early inflammatory response to full-thickness skin wounding, thereby providing *in vivo* relevance of

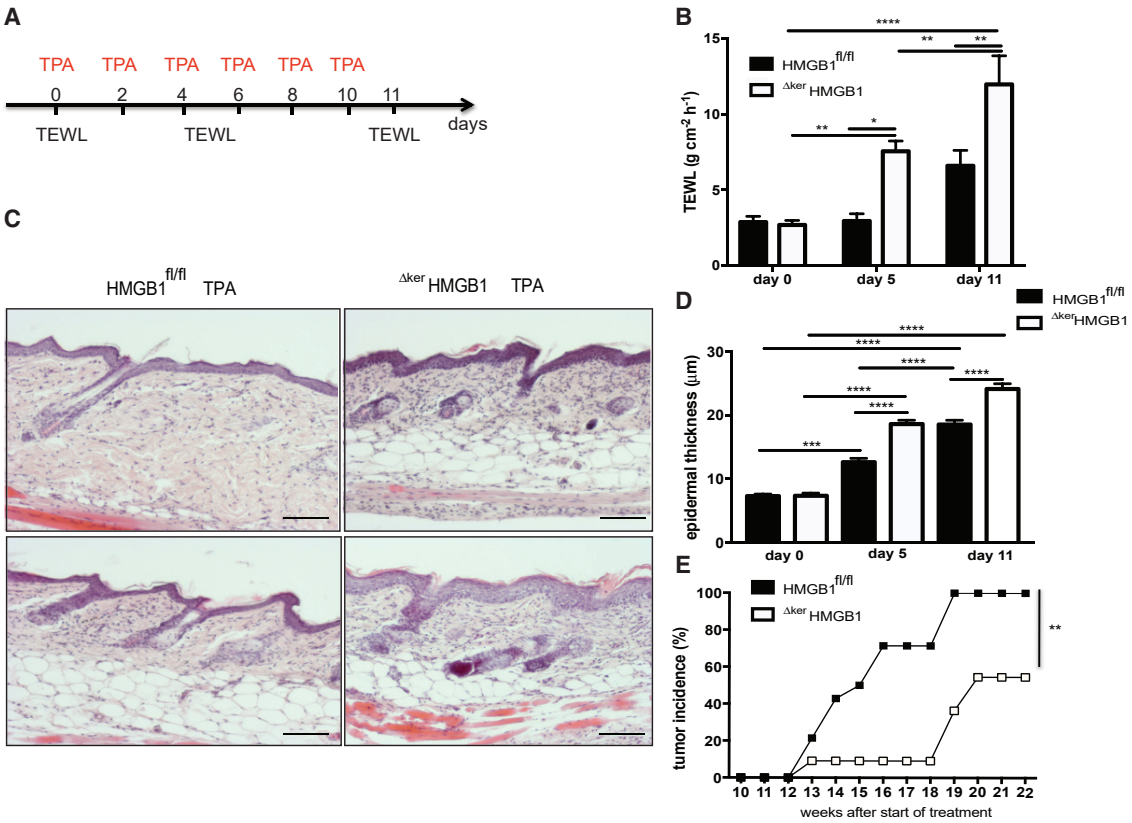

Figure 2. Keratinocyte-Specific HMGB1-Deficient Mice Exhibit an Exacerbated Response to TPA Treatment but Are Protected from DMBA-Induced Carcinogenesis

(A) Experimental outline of TPA barrier perturbation protocol.

(B) Transepidermal water loss (TEWL) measurements were recorded 24 h after the last TPA treatment in HMGB1$^{fl/fl}$ (n = 8) and Δ^{Ker} HMGB1 (n = 14) mice (****p < 0.0001; **p ≤ 0.01; *p ≤ 0.05; two-way ANOVA with multiple comparisons). Data represent mean ± SEM.

(C) Representative H&E-stained skin sections from HMGB1$^{fl/fl}$ and Δ^{Ker} HMGB1 mice that were subjected to six topical applications of TPA. Scale bars: 50 μm.

(D) Epidermal thickness was measured on H&E sections by ImageJ software; 10 measurements per field were performed for 3 fields per mouse. The thickness of the epidermis was determined by measuring the distance from the basement membrane to the upper granular layer, excluding the cornified layers (****p < 0.0001; ***p = 0.0001; two-way ANOVA with multiple comparisons)). Data represent mean ± SEM.

(E) Tumor incidence (% of mice with one or more tumors) in HMGB1$^{fl/fl}$ (n = 14) and Δ^{Ker} HMGB1 (n = 11) mice treated with DMBA (**p = 0.002; Wilcoxon matched-pairs signed rank test).

See also Figure S2.

HMGB1 acting as an upstream regulator of NET formation in skin reparative inflammation.

Altered NET Formation Impacts on Wound-Induced Tumorigenesis

The increased presence of NETs, delaying regenerative responses in skin, has recently been described in the context of diabetes (Menegazzo et al., 2015; Wong et al., 2015). To investigate whether ablation of HMGB1 in keratinocytes affects wound-induced tumor formation in conditions where neutrophils are primed to NET formation, we subjected InvEE Δ^{Ker} HMGB1 and InvEE HMGB1$^{fl/fl}$ mice to streptozotocin (STZ)-induced type 1 diabetes. STZ-challenged InvEE Δ^{Ker} HMGB1 diabetic mice developed wound-induced tumor formation with an incidence comparable to that of InvEE HMGB1$^{fl/fl}$ mice (Figure 4A), indicating that in conditions that predispose neutrophils to NET formation, lack of epithelial-derived HMGB1 is no longer capable of protecting the skin from tumorigenesis. This acquired sensitivity to tumor development correlated with a less prominent reduction in NET formation in wounded STZ-induced Δ^{Ker} HMGB1 diabetic mice relative to wounded STZ-induced wild-type diabetic mice, as demonstrated by western blotting for H3^{citr} levels (Figure 4B).

Digestion of NETs by DNase1 is sufficient to accelerate their clearance by macrophages (Farrera and Fadeel, 2013). To assess the causative involvement of NETs in cutaneous wound-induced tumorigenesis, we next investigated whether inhibiting NETs by injecting DNase1 in InvEE mice could alter skin tumor susceptibility. Indeed, injection of DNase1 in HMGB1-proficient InvEE mice at the time of wounding and in the initial stages of wound healing resulted in a significant protection from wound-induced tumorigenesis (Figure 4C). In agreement, a significant

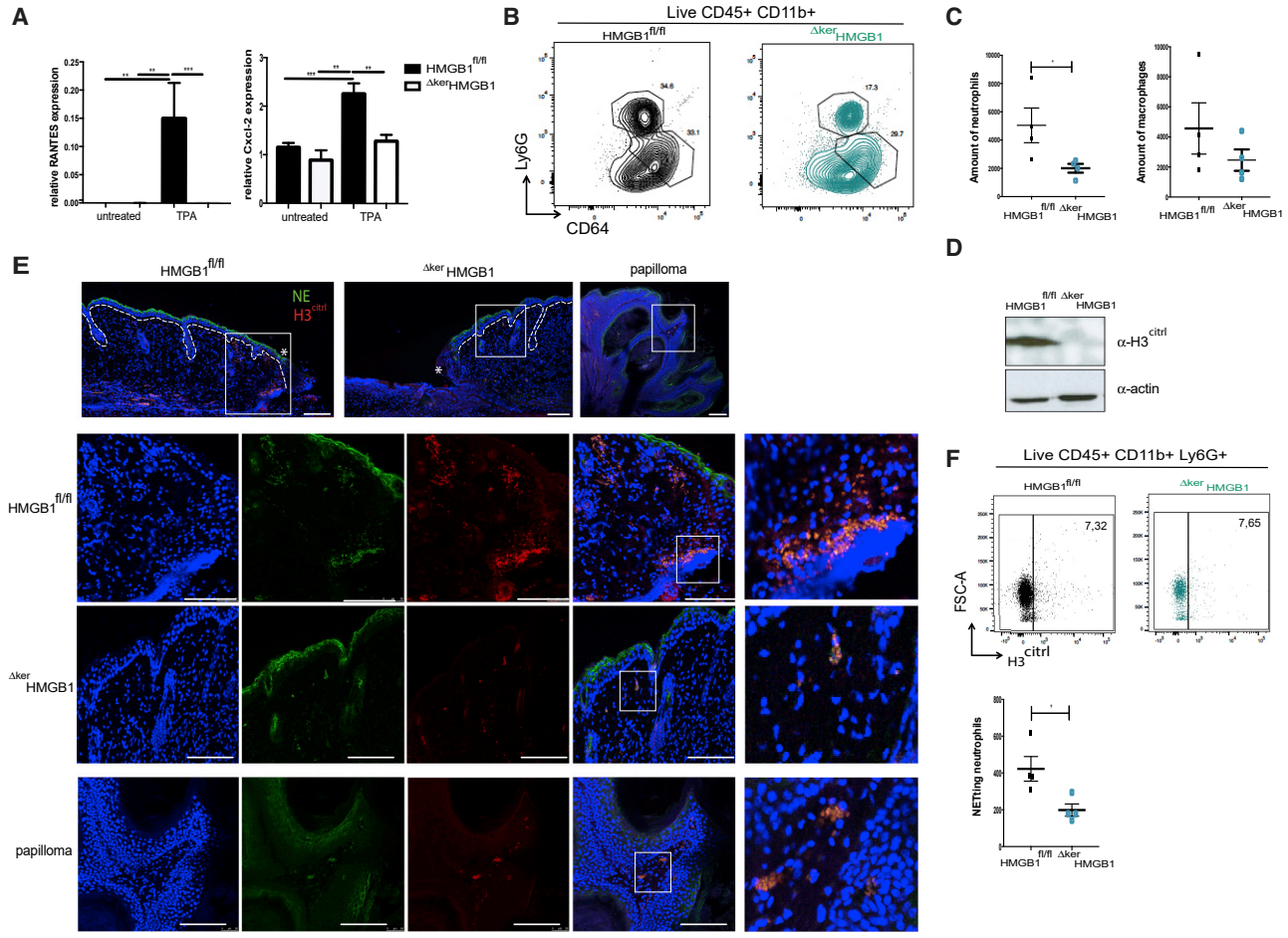

Figure 3. Keratinocyte-Derived HMGB1 Promotes Neutrophil Infiltration and NET Formation in Skin Wounds

(A) Relative levels of *Rantes* and *Cxcl2* in epidermal lysates from TPA-treated HMGB1$^{fl/fl}$ and Δ^{Ker} HMGB1 skin. Data are depicted as the ratio of the mRNA expression normalized to GAPDH and expressed as mean ± SEM (n = 4 per condition; **p = 0.0023; ***p = 0.0007; two-way ANOVA with multiple comparisons).

(B) Expression of CD64 and Ly6G by live CD45+ CD11b+ cells in skin wounds of HMGB1$^{fl/fl}$ and Δ^{Ker} HMGB1 mice.

(C) Absolute number of neutrophils and macrophages per skin wound at day 2 post-wounding in HMGB1$^{fl/fl}$ and Δ^{Ker} HMGB1 mice (n = 4 per group; *p = 0.0286; Mann-Whitney test).

(D) Western blotting for citrullinated histone-3 (H3^{citr}) on skin lysates of wounds at day 2 post-wounding in HMGB1$^{fl/fl}$ and Δ^{Ker} HMGB1 mice. α-actin blot is shown as loading control.

(E) Immunofluorescent labeling of neutrophil extracellular traps in skin wounds of HMGB1$^{fl/fl}$ and Δ^{Ker} HMGB1 mice and in wound-induced InvEE papillomas. Paraffin sections were stained with antibodies against neutrophil elastase (NE; green), citrullinated histone-3 (H3^{citr}; red), and DAPI (blue) as nuclear counterstain. Scale bars: 100 μm. Dotted line represents epidermal-dermal boundary, asterisk indicates the wound edge, and boxed areas are magnifications as shown in the boxes below and in the right panels.

(F) Presence of citrullinated histone-3 by live CD45+ CD11b+ Ly6G+ neutrophils in skin wounds of HMGB1$^{fl/fl}$ and Δ^{Ker} HMGB1 mice at day 2 post-wounding. Absolute cell numbers of netting neutrophils per skin wound at day 2 post-wounding in HMGB1$^{fl/fl}$ and Δ^{Ker} HMGB1 mice (n = 4 per group; *p = 0.0286; Mann-Whitney test).

reduction in H3^{citr} levels could be observed in wound lysates after DNase1 treatment (Figure 4D). DNase1-injected mice also closed their wounds markedly faster than control-injected InvEE HMGB1$^{fl/fl}$ mice (Figure 4E), recapitulating the effect of HMGB1 ablation from keratinocytes. Interestingly, DNase 1 treatment did not alter wound healing rates in Δ^{Ker} HMGB1 mice (Figure S3A). Of note, when epithelial damage was induced in InvEE HMGB1-proficient mice by repetitive topical TPA treatment, NETs could not be observed, and this type of injury did not result in tumor formation in InvEE mice (Figure 4F; Figure S3B), demonstrating that the formation of NETs occurs only in specific conditions of epithelial damage where it can drive tumor initiation.

HMGB1 Secretion and the Presence of NETs Coincide in Wounded and Tumor-Bearing Skin

Our previous study demonstrated HMGB1 secretion in wound-induced tumors in mice as well as in patients suffering from the skin blistering disease RDEB (Hoste et al., 2015). Immunofluorescent analysis revealed that HMGB1 is indeed highly upregulated in the murine wound and tumor microenvironment from

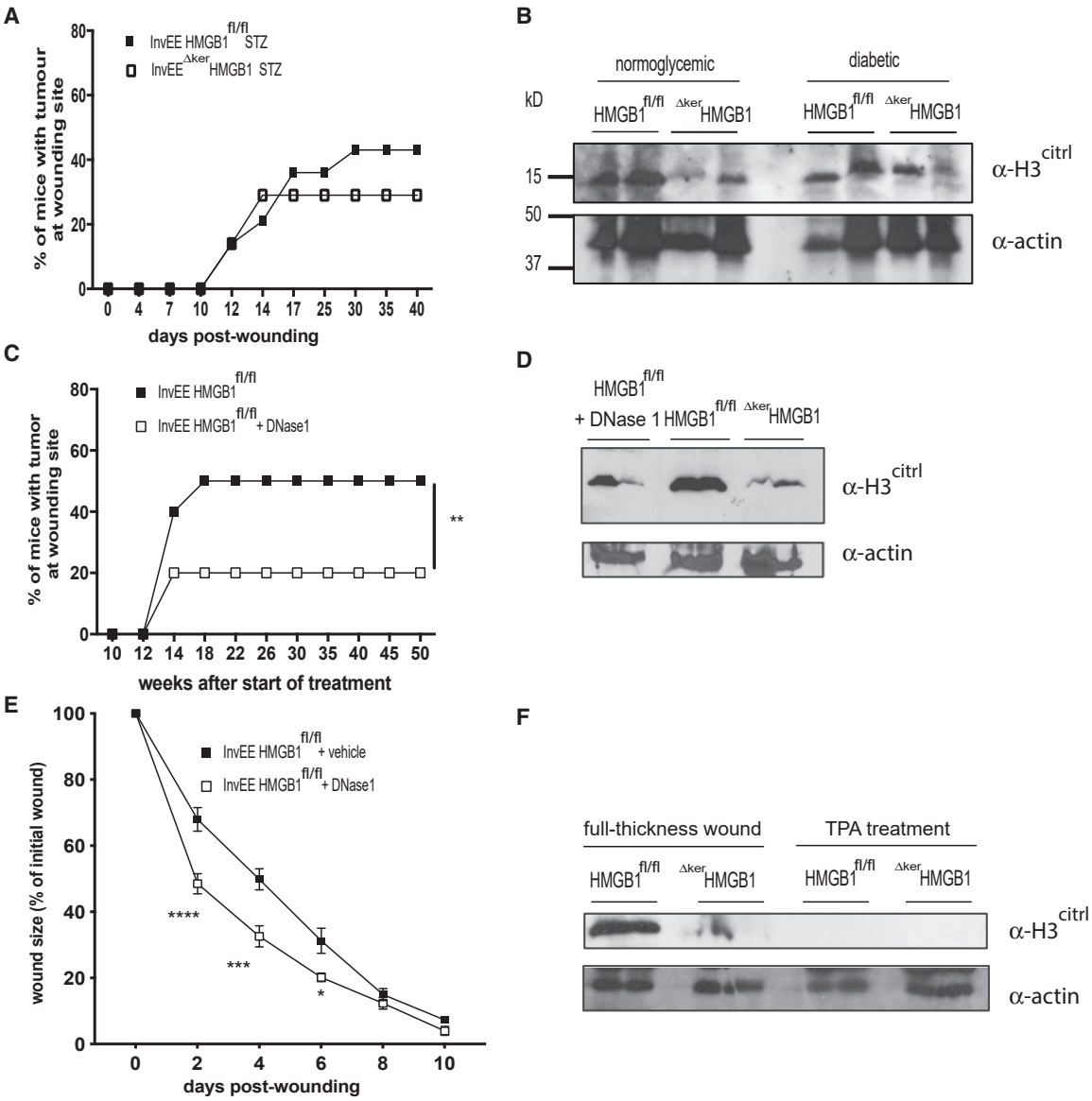

Figure 4. Altering NET Levels Impacts on Wound-Induced Tumorigenesis

(A) Wound-induced skin tumor incidence in STZ-challenged InvEE HMGB1$^{fl/fl}$ (n = 14) and InvEE Δ^{Ker} HMGB1 (n = 7) diabetic mice (ns, Wilcoxon matched-pairs signed rank test).

(B) Western blotting for H3^{citr} on skin lysates of wounds at day 2 post-wounding in normoglycemic and STZ-induced InvEE diabetic mice. α-actin blot is shown as loading control.

(C) Wound-induced skin tumor incidence in InvEE HMGB1$^{fl/fl}$ mice injected with the NET inhibitor DNase 1 (n = 10) or with vehicle (PBS; n = 10) at time of wounding and 12, 24, and 36 h post-wounding (**p = 0.002; Wilcoxon matched-pairs signed rank test).

(D) Western blotting for H3^{citr} on skin lysates of wounds at day 2 post-wounding in InvEE Δ^{Ker} HMGB1 and control mice injected with DNase 1 or PBS (vehicle). α-actin blot is shown as loading control.

(E) Wound healing dynamics of InvEE HMGB1$^{fl/fl}$ mice injected with DNase 1 (n = 11) or PBS (vehicle; n = 20) (****p < 0.0001; ***p = 0.0001; *p = 0.0415; two-way ANOVA with multiple comparisons). Data represent mean ± SEM.

(F) Western blotting for H3^{citr} on skin lysates of InvEE wounds at day 2 post-wounding or on lysates of TPA-treated skin of HMGB1$^{fl/fl}$ and Δ^{Ker} HMGB1 mice. α-actin blot is shown as loading control.

See also Figure S3.

control HMGB1$^{fl/fl}$ mice (Figure 5A). At day 2 post-wounding, we observed the highest expression of HMGB1, both in the wound stroma and in the adjacent epidermis (Figure 5A). Residual HMGB1 staining in Δ^{Ker} HMGB1 epidermis is likely due to HMGB1 expression by epidermal-resident immune cells. At day 14 post-wounding, when re-epithelialization is largely

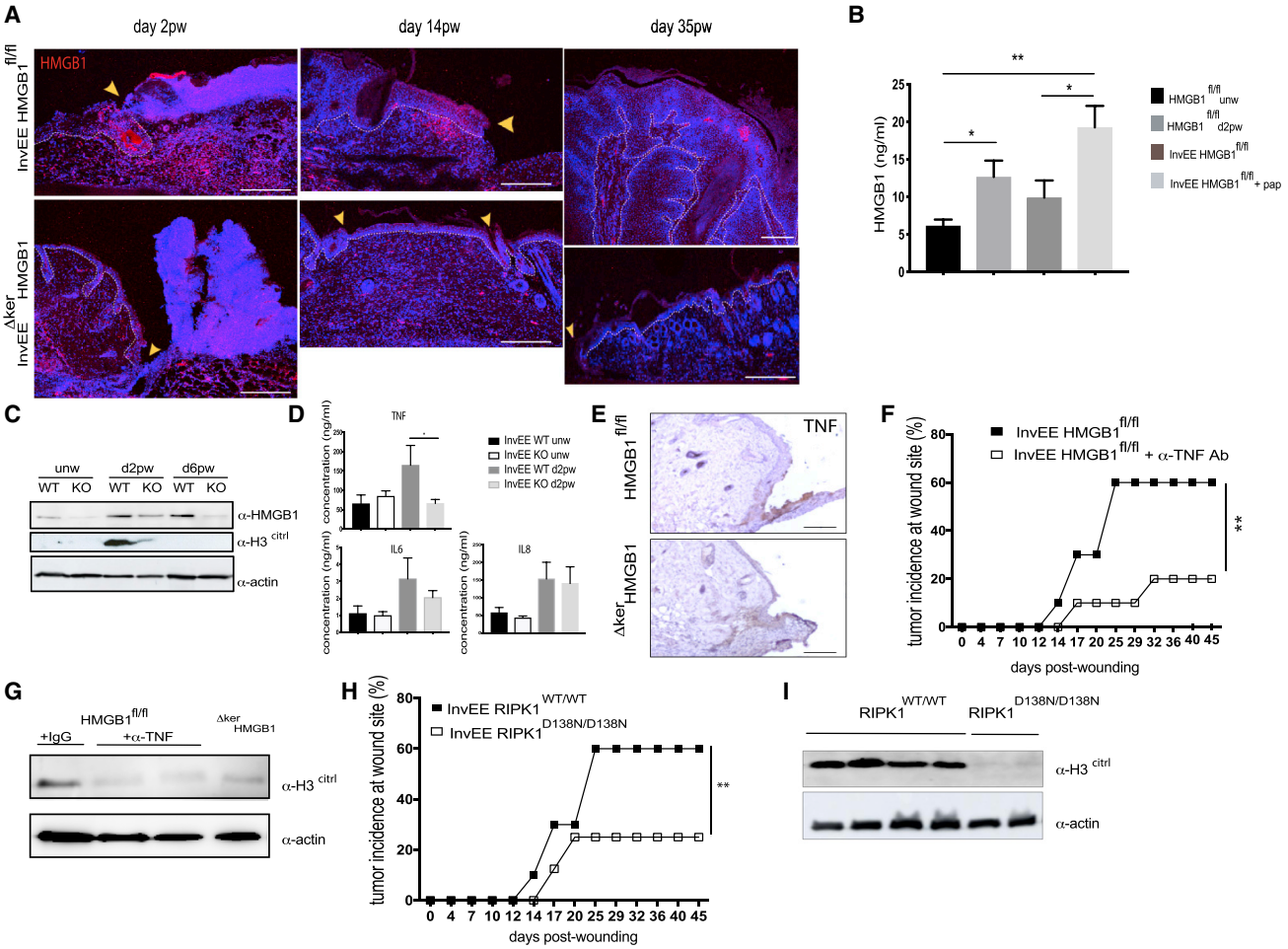

Figure 5. Keratinocyte-Specific HMGB1 Mediates Regenerative and Tumorigenic Responses through TNF and RIPK1 Kinase Activity

(A) Paraffin sections of wounded and tumor-bearing InvEE HMGB1$^{fl/fl}$ and Δ^{Ker} HMGB1 skin were labeled with an anti-HMGB1 (red) antibody and counterstained with DAPI (blue). Scale bars: 200 μm. dpw, days post-wounding. Arrowheads indicate the wound edge.

(B) Serum levels of HMGB1 in unwounded, wounded (d2pw, day 2 post-wounding), inflamed (InvEE), and InvEE mice bearing a wound-induced papilloma, as assessed by ELISA (data represent mean ± SEM; n ≥ 4 per condition; *p < 0.05; **p = 0.0012; Mann-Whitney test).

(C) Western blotting for HMGB1 and H3^{citr} in skin lysates of unwounded (unw), and wounded (day 2, 6, and 8 post-wounding [pw]) InvEE HMGB1$^{fl/fl}$ (wild-type [WT]) and Δ^{Ker} HMGB1 (knockout [KO]) mice. α-actin blot is shown as loading control.

(D) Concentration of TNF, IL-6, and IL-8 in serum of unwounded and wounded InvEE HMGB1$^{fl/fl}$ (WT) and Δ^{Ker} HMGB1 (KO) mice (data represent mean ± SEM; n ≥ 4 per condition; *p = 0.0317; Mann-Whitney test).

(E) Staining for TNF in wounded skin of InvEE HMGB1$^{fl/fl}$ and Δ^{Ker} HMGB1 mice at day 2 post-wounding. Scale bars: 50 μm.

(F) Wound-induced tumor incidence in InvEE HMGB1$^{fl/fl}$ mice intradermally injected with control IgG (n = 10) or TNF antagonistic antibody (n = 10) at time of wounding and 12, 24, and 36 h post-wounding (**p = 0.002; Wilcoxon matched-pairs signed rank test).

(G) Western blotting for H3^{citr} of day 2 post-wounding skin lysates of Δ^{Ker} HMGB1 and HMGB1$^{fl/fl}$ mice injected with α-TNF or α-IgG control antibodies. α-actin blot is shown as loading control.

(H) Wound-induced skin tumor incidence in InvEE RIPK1$^{WT/WT}$ mice (n = 10) and InvEE RIPK1$^{D138N/D138N}$ mice (n = 10) (**p = 0.0039; Wilcoxon matched-pairs signed rank test).

(I) Western blotting for H3^{citr} of day 2 post-wounding skin lysates of InvEE RIPK1$^{D138N/D138N}$ and InvEE RIPK1$^{WT/WT}$ mice. α-actin blot is shown as loading control.

completed, HMGB1 was still prevalent in wounded epidermis and underlying stroma of HMGB1$^{fl/fl}$ mice, albeit to a lesser extent than at day 2 post-wounding (Figure 5A). We further observed higher levels of circulating HMGB1 levels in serum from wounded mice compared to unwounded mice, and these levels were even higher in serum of mice bearing skin tumors (Figure 5B).

The enhanced expression of HMGB1 in wounded skin was next confirmed by western blotting on HMGB1$^{fl/fl}$ wound lysates (Figure 5C), and a significantly reduced HMGB1 expression could be confirmed in Δ^{Ker} HMGB1 skin wounds compared to HMGB1$^{fl/fl}$ controls, demonstrating that keratinocytes are the main source of HMGB1 during wound healing responses. The prominent upregulation of HMGB1 during the early

post-wounding stage coincided with the highest expression of $H3^{citr}$ (Figure 5C), implicating the formation of NETs as an early and transient response to wounding. Interestingly, this early post-wounding time point also represents the period when most striking differences in wound healing responses are observed between keratinocyte-specific HMGB1-proficient versus -deficient mice (Figures 1A and 1B), indicating that HMGB1 induces the release of NETs mainly in the initial stages of wound healing, where they hamper regeneration and induce neoplastic events.

Keratinocyte-Specific HMGB1 Mediates Regenerative and Tumorigenic Responses through TNF and RIPK1 Kinase Activity

The proinflammatory cytokine TNF was previously shown to promote chemically induced skin carcinogenesis (Moore et al., 1999). To examine whether TNF mediates cutaneous regenerative and tumorigenic responses downstream of HMGB1, we assessed the levels of TNF in circulation of wounded and unwounded InvEE Δ^{Ker} HMGB1 mice relative to InvEE HMGB1-proficient mice. Interestingly, a marked reduction in serum levels of TNF was observed in wounded InvEE Δ^{Ker} HMGB1 mice relative to wounded InvEE HMGB1-proficient mice, while the levels of other proinflammatory cytokines that are known to be involved in skin carcinogenesis, such as IL (interleukin)-6 and IL-8 levels, were not significantly altered between wounded mice of both genotypes (Figure 5D). In agreement, staining for TNF in cutaneous wounds of InvEE Δ^{Ker} HMGB1 and control mice confirmed reduced levels of TNF in wounds of mice lacking HMGB1 from keratinocytes (Figure 5E). Finally, TNF-blocking antibodies were injected in InvEE mice during the early post-wounding stage, demonstrating a significant reduction in wound-induced tumor formation compared to immunoglobulin G (IgG)-injected control mice (Figure 5F). Western blotting of wound lysates of InvEE mice treated with and without TNF-blocking antibodies revealed that $H3^{citr}$ levels were markedly reduced upon inhibition of TNF (Figure 5G).

Recent work demonstrated that neutrophil Receptor-Interacting-Protein Kinase-1 (RIPK1)-dependent necroptosis drives NET formation (D'Cruz et al., 2018). Since TNF mediates RIPK1-dependent apoptosis and necroptosis, we next investigated whether wound-induced tumor formation depends on the kinase function of RIPK1. For this, kinase-dead RIPK1 ($RIPK1^{D138N}$) mutant mice (Polykratis et al., 2014) were generated in the InvEE genetic background, wounded, and monitored for skin papillomagenesis. InvEE $RIPK1^{D138N}$ mice were strongly protected from wound-induced tumor development, demonstrating that RIPK1 kinase activity drives tumor formation (Figure 5H). Western blotting of wounded skin lysates confirmed that citrullination of histone-3 could not be observed in the absence of RIPK1 kinase activity (Figure 5I). In conclusion, these data show that TNF and subsequent RIPK1 activity act downstream of HMGB1 to mediate NET formation and cutaneous tumor formation.

HMGB1 Secretion by Human SCC Cells Induces Cell Death in Neutrophils

To investigate the relevance of enhanced HMGB1 expression for NET formation and tumor induction in human skin, we analyzed skin sections from RDEB patients. Immunofluorescent analysis of tissue sections obtained from RDEB patients demonstrated the presence of NETs in RDEB lesional and SCC-associated skin (Figure 6A), indicating that also in human skin, tumorigenicity of the wound microenvironment can be associated with the occurrence of NETs. To further validate this hypothesis, we analyzed the levels of secreted HMGB1 in the supernatant of normal human keratinocyte cell lines versus SCC cells and could observe a significant increase in HMGB1 release in SCC keratinocytes versus normal keratinocytes (Figure 6B). Finally, live imaging of human neutrophils incubated with conditioned medium of SCC versus normal keratinocytes revealed that neutrophil death is accelerated upon incubation of the cells with conditioned medium from SCC keratinocytes compared to conditioned medium from normal keratinocytes (Figures 6C and 6D).

Together, these data identify a crucial role for epithelial-derived HMGB1 in driving tumorigenicity of cutaneous wounds by mediating the levels of NET formation by skin-infiltrating neutrophils in the early stages of wound repair. Upon pharmacological inhibition of HMGB1 or NET formation in this early post-wounding stage, mice close their cutaneous wounds faster and are fully protected from keratinocyte-derived tumor initiation.

DISCUSSION

Regenerative inflammation can induce neoplastic responses; however, the molecular mechanisms underlying this association are largely unknown. Our data identified a crucial role for keratinocyte-derived HMGB1 in delaying cutaneous injury repair and in driving tumorigenicity of cutaneous wounds by mediating neutrophilic inflammation and NET formation in the early stages of wound repair. Mice close their cutaneous wounds faster and are fully protected from keratinocyte-derived tumor initiation when HMGB1 release or NET formation are prevented in the early post-wounding stage, suggesting that targeting HMGB1 or NETs might represent an interesting therapeutic avenue in reducing wound-associated skin tumorigenesis.

Neutrophils represent the main cell type involved in the early immune response during injury repair, where they can produce NETs that have recently been implicated in various infectious and inflammatory pathologies, including sepsis, liver injury, atherosclerosis, and asthma (Hernandez et al., 2018; Papayannopoulos, 2018; Toussaint et al., 2017; Warnatsch et al., 2015). NETs can exert beneficial effects on wound healing due to their bactericidal effects (Li et al., 2010; Brinkmann et al., 2004). However, antimicrobial factors such as neutrophil elastase and histones can also damage epithelia and delay wound healing, as is seen in conditions of excessive NET formation (Dovi et al., 2003; Wong et al., 2015). Interestingly, the differences in wound healing rates observed in Δ^{Ker} HMGB1 mice versus control mice are most obvious during the time frame in which NET formation occurs (Figures 1, 3, and 5).

TNF also has a predominant damaging activity in wound healing and skin tumorigenesis and is highly potent in priming neutrophils. Our observation that both TNF neutralization as well as genetic inactivation of RIPK1 kinase activity protects mice from wound-induced tumorigenesis indicates a crucial role for

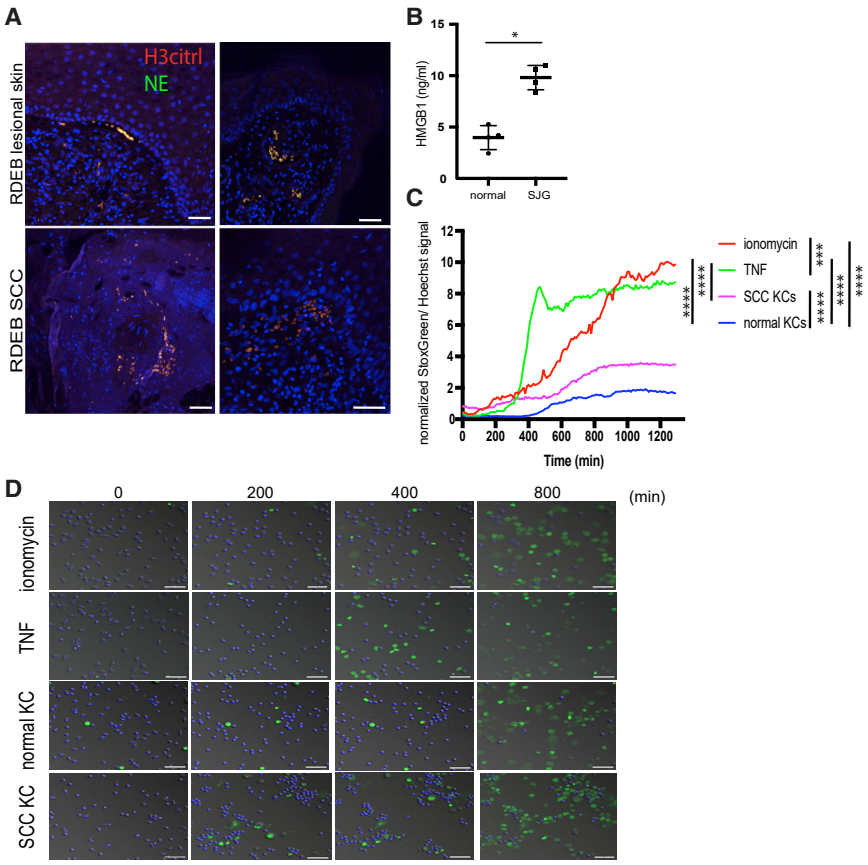

Figure 6. HMGB1 Secretion by SCC Keratinocytes Induces Neutrophilic Cell Death

(A) Immunofluorescent labeling of NETs in lesional skin and SCCs of RDEB patients. Paraffin sections were stained with antibodies against neutrophil elastase (NE; green), citrullinated histone-3 ($H3^{citr}$; red), and DAPI (blue) as nuclear counterstain. Scale bars: 50 μm.

(B) HMGB1 levels in supernatant of normal and SCC human keratinocytes cultured in serum-free conditions.

(C) Quantification of DNA externalization in response to incubation with different conditioned media as assessed by the ratio of Sytox Green over Hoechst over time in live imaging of human neutrophils (n = 6 per condition; ****p < 0.0001; ***p = 0.0001; two-way ANOVA with multiple comparisons). Stimulation with recombinant TNF and ionomycin was used as a positive control.

(D) DNA externalization as assessed by live imaging. Human neutrophils were stained with Hoechst (blue) and DNA externalization was assessed by SytoxGreen (green) positivity at the indicated time points. Scale bar: 50 μm. Data represent mean ± SEM.

HMGB1 in driving TNF-RIPK1 signaling to skin carcinogenesis (Figure 5). This is in line with a previous report indicating that antibody-mediated depletion of HMGB1 in a model of LPS-induced lung inflammation dampened TNF-release and reduced NET formation (Tadie et al., 2013).

Several molecular signaling pathways lead to the formation of NETs (Konig and Andrade, 2016). One of these pathways was initially described by Zychlinski et al. and shown to be dependent on Nox2-mediated reactive oxygen species (ROS) production (Brinkmann et al., 2004; Fuchs et al., 2007). An alternative and presumably antagonistic pathway of chromatin extrusion by neutrophils relies on calcium-dependent PAD4-mediated hypercitrullination (Wang et al., 2009). More recently, RIPK1-mediated necroptosis (Desai et al., 2016) and gasdermin D-mediated (Chen et al., 2018) pore formation were also shown to facilitate the release of NETs. Our data identify a crucial role for NET formation associated with protein hypercitrullination in skin wounding and tumor initiation, consistent with an earlier study demonstrating NET accumulation in diabetic skin wounds (Wong et al., 2015). Staining for NETs in wounded and tumor-bearing skin clearly showed reduced NET formation in the absence of keratinocyte-derived HMGB1 (Figure 3E). We cannot exclude additional NET-independent effects of keratinocyte-derived HMGB1 on neutrophil function. Indeed, decreased neutrophil infiltration in Δ^{Ker} HMGB1 mice is in accordance with the role of HMGB1 as a cytokine. We hypothesize that HMGB1 critically contributes to exceeding the inflammatory threshold by the recruitment of neutrophils and the formation of NETs, thereby creating an inflammatory milieu that in turn favors NET formation. However, the direct and critical involvement of NETs was apparent from the tumor-protective and accelerated regenerative effect of DNase1 treatment during early post-wounding stages (Figures 4C and 4E).

NET formation has been documented in murine breast cancer tumors, and metastatic cancer cells can induce NETs, thereby promoting cancer dissemination (Park et al., 2016). NET formation through neutrophil priming has also been shown to favor tumor growth (Demers et al., 2016), together suggesting the importance of NET formation for cancer. Our study proves that the initial burst of NET formation caused by epithelial injury in the skin critically promotes tumor initiation and is mediated by epithelial-derived HMGB1 release.

Our observations in RDEB patients, in which we demonstrate the presence of NETs in lesional skin and SCCs (Figure 6A), indicate that these molecular events are relevant to human disease. We propose that anti-HMGB1, anti-TNF, or anti-NET therapies might be of particular interest in such patients, as well as in wound care of diabetic patients suffering from chronic ulcers, since these therapies could ameliorate wound healing responses, while limiting the risk of cutaneous tumorigenicity. Finally, this newly identified role of HMGB1 in mediating tumorigenicity of wounds through NET formation might well represent a signaling cascade that impacts on other barrier tissues where trauma is linked to tumor formation, such as in lung, liver, or the intestine, suggesting that HMGB1 targeting or prevention of NET formation might also be beneficial as a therapy in such disease conditions.

STAR★METHODS

Detailed methods are provided in the online version of this paper and include the following:

- KEY RESOURCES TABLE
- LEAD CONTACT AND MATERIALS AVAILABILITY
- EXPERIMENTAL MODEL AND SUBJECT DETAILS
  - Mice
  - Isolation and culture conditions of keratinocytes
  - Study approval
- METHOD DETAILS
  - Wound healing assays and wound-induced tumor formation
  - Chemical carcinogenesis protocols
  - Induction of type 1 diabetes by streptozotocin injections
  - Immunofluorescence
  - Immunohistochemistry
  - Western blotting
  - Flow cytometry
  - Recombinant mHMGB1 A-box expression and purification
  - Primary keratinocyte cultures and scratch-wound assays
  - RNA isolation and qPCR
  - Cytokine measurements
  - RNA sequencing and bioinformatics
  - Isolation of polymorphonuclear leukocytes
  - Live Cell Imaging
- QUANTIFICATION AND STATISTICAL ANALYSIS
- DATA AND CODE AVAILABILITY

SUPPLEMENTAL INFORMATION

Supplemental Information can be found online at https://doi.org/10.1016/j.celrep.2019.10.104.

ACKNOWLEDGMENTS

We thank Ruben Van Renterghem and Sabine Cleemput for animal care and acknowledge the VIB BioImaging Core, the VIB Nucleomics Core, the VIB FlowCore, and Gert Van Isterdael for technical assistance. TLR-4 blocking antibody was kindly provided by Dr. Walter Ferlin. We thank Manolis Pasparakis for providing RIPK1^{D138N} mice and all members of the van Loo laboratory for suggestions and discussions. E.H. is supported by an FWO postdoctoral fellowship. L.v.H. holds an FWO FR fellowship. Research in the van Loo lab is supported by research grants from the FWO, the Concerted Research Actions (GOA) of Ghent University, the Geneeskundige Stichting Koningin Elisabeth (GSKE), Stichting tegen Kanker, the CBC Banque prize, the Charcot Foundation, the Belgian Foundation against Cancer, and Kom op tegen Kanker. C.M. is supported by a postdoctoral research fellowship from the German Research Foundation (DFG) (MA 7770/1-1). We are grateful for the courtesy of Peter Vandenabeele to deliver purified HMGB1 in the framework of a Methusalem grant (BOF16/MET_V/007). W.D. lab is supported by Stichting tegen Kanker (FAF-F/2016/868). I.F. is funded by FONDECYT (1181093). K.R. is supported by an Odysseus grant and ERC Advanced Grant.

AUTHOR CONTRIBUTIONS

E.H. conceptualized the study, designed and performed experiments, and analyzed the data. C.M., L.v.H., L.C., and H.-K.V. performed experiments. I.F., F.P., S.G., and J.C.S.-A. provided skin tissue sections from normal and RDEB patients. B.M., A.G., and E.P. performed and analyzed live imaging experiments. R.R. and W.D. provided ultrapure Box A protein. D.K. and K.W.M. provided supernatants from human cell lines. L.B. provided anti-TNF antibody. P.H. and R.F.S. provided the "floxed" HMGB1 mice. L.C., L.M., Y.S., K.R., and G.v.L. analyzed the data and provided input for experimental design. E.H., C.M., and G.v.L. wrote the manuscript with input from all authors.

DECLARATION OF INTERESTS

The authors declare no competing interests.

Received: January 14, 2019
Revised: September 6, 2019
Accepted: October 25, 2019
Published: November 26, 2019

REFERENCES

Abel, E.L., Angel, J.M., Kiguchi, K., and DiGiovanni, J. (2009). Multi-stage chemical carcinogenesis in mouse skin: fundamentals and applications. Nat. Protoc. *4*, 1350–1362.

Arwert, E.N., Lal, R., Quist, S., Rosewell, I., van Rooijen, N., and Watt, F.M. (2010). Tumor formation initiated by nondividing epidermal cells via an inflammatory infiltrate. Proc. Natl. Acad. Sci. USA *107*, 19903–19908.

Arwert, E.N., Hoste, E., and Watt, F.M. (2012). Epithelial stem cells, wound healing and cancer. Nat. Rev. Cancer *12*, 170–180.

Belaaouaj, A., McCarthy, R., Baumann, M., Gao, Z., Ley, T.J., Abraham, S.N., and Shapiro, S.D. (1998). Mice lacking neutrophil elastase reveal impaired host defense against gram negative bacterial sepsis. Nat. Med. *4*, 615–618.

Boeltz, S., Amini, P., Anders, H.J., Andrade, F., Bilyy, R., Chatfield, S., Cichon, I., Clancy, D.M., Desai, J., Dumych, T., et al. (2019). To NET or not to NET:current opinions and state of the science regarding the formation of neutrophil extracellular traps. Cell Death Differ. *26*, 395–408.

Brinkmann, V., Reichard, U., Goosmann, C., Fauler, B., Uhlemann, Y., Weiss, D.S., Weinrauch, Y., and Zychlinsky, A. (2004). Neutrophil extracellular traps kill bacteria. Science *303*, 1532–1535.

Chen, K.W., Monteleone, M., Boucher, D., Sollberger, G., Ramnath, D., Condon, N.D., von Pein, J.B., Broz, P., Sweet, M.J., and Schroder, K. (2018). Noncanonical inflammasome signaling elicits gasdermin D-dependent neutrophil extracellular traps. Sci. Immunol. *3*, eaar6676.

Clausen, B.E., Burkhardt, C., Reith, W., Renkawitz, R., and Förster, I. (1999). Conditional gene targeting in macrophages and granulocytes using LysMcre mice. Transgenic Res. *8*, 265–277.

D'Cruz, A.A., Speir, M., Bliss-Moreau, M., Dietrich, S., Wang, S., Chen, A.A., Gavillet, M., Al-Obeidi, A., Lawlor, K.E., Vince, J.E., et al. (2018). The pseudokinase MLKL activates PAD4-dependent NET formation in necroptotic neutrophils. Sci. Signal. *11*, eaao1716.

Davé, S.H., Tilstra, J.S., Matsuoka, K., Li, F., DeMarco, R.A., Beer-Stolz, D., Sepulveda, A.R., Fink, M.P., Lotze, M.T., and Plevy, S.E. (2009). Ethyl pyruvate decreases HMGB1 release and ameliorates murine colitis. J. Leukoc. Biol. *86*, 633–643.

Degryse, B., Bonaldi, T., Scaffidi, P., Müller, S., Resnati, M., Sanvito, F., Arrigoni, G., and Bianchi, M.E. (2001). The high mobility group (HMG) boxes of the nuclear protein HMG1 induce chemotaxis and cytoskeleton reorganization in rat smooth muscle cells. J. Cell Biol. *152*, 1197–1206.

Demers, M., Wong, S.L., Martinod, K., Gallant, M., Cabral, J.E., Wang, Y., and Wagner, D.D. (2016). Priming of neutrophils toward NETosis promotes tumor growth. OncoImmunology *5*, e1134073.

Desai, J., Kumar, S.V., Mulay, S.R., Konrad, L., Romoli, S., Schauer, C., Herrmann, M., Bilyy, R., Müller, S., Popper, B., et al. (2016). PMA and crystal-induced neutrophil extracellular trap formation involves RIPK1-RIPK3-MLKL signaling. Eur. J. Immunol. *46*, 223–229.

Dovi, J.V., He, L.K., and DiPietro, L.A. (2003). Accelerated wound closure in neutrophil-depleted mice. J. Leukoc. Biol. *73*, 448–455.

Farrera, C., and Fadeel, B. (2013). Macrophage clearance of neutrophil extracellular traps is a silent process. J. Immunol. *191*, 2647–2656.

Fine, J.D., Johnson, L.B., Weiner, M., Li, K.P., and Suchindran, C. (2009). Epidermolysis bullosa and the risk of life-threatening cancers: the National EB Registry experience, 1986-2006. J. Am. Acad. Dermatol. *60*, 203–211.

Fuchs, T.A., Abed, U., Goosmann, C., Hurwitz, R., Schulze, I., Wahn, V., Weinrauch, Y., Brinkmann, V., and Zychlinsky, A. (2007). Novel cell death program leads to neutrophil extracellular traps. J. Cell Biol. *176*, 231–241.

Hernandez, C., Huebener, P., and Schwabe, R.F. (2016). Damage-associated molecular patterns in cancer: a double-edged sword. Oncogene *35*, 5931–5941.

Hernandez, C., Huebener, P., Pradere, J.P., Antoine, D.J., Friedman, R.A., and Schwabe, R.F. (2018). HMGB1 links chronic liver injury to progenitor responses and hepatocarcinogenesis. J. Clin. Invest. *128*, 2436–2451.

Hobbs, R.M., Silva-Vargas, V., Groves, R., and Watt, F.M. (2004). Expression of activated MEK1 in differentiating epidermal cells is sufficient to generate hyperproliferative and inflammatory skin lesions. J. Invest. Dermatol. *123*, 503–515.

Hori, O., Brett, J., Slattery, T., Cao, R., Zhang, J., Chen, J.X., Nagashima, M., Lundh, E.R., Vijay, S., Nitecki, D., et al. (1995). The receptor for advanced glycation end products (RAGE) is a cellular binding site for amphoterin. Mediation of neurite outgrowth and co-expression of rage and amphoterin in the developing nervous system. J. Biol. Chem. *270*, 25752–25761.

Hoste, E., Arwert, E.N., Lal, R., South, A.P., Salas-Alanis, J.C., Murrell, D.F., Donati, G., and Watt, F.M. (2015). Innate sensing of microbial products promotes wound-induced skin cancer. Nat. Commun. *6*, 5932.

Huebener, P., Gwak, G.Y., Pradere, J.P., Quinzii, C.M., Friedman, R., Lin, C.S., Trent, C.M., Mederacke, I., Zhao, E., Dapito, D.H., et al. (2014). High-mobility group box 1 is dispensable for autophagy, mitochondrial quality control, and organ function in vivo. Cell Metab. *19*, 539–547.

Huebener, P., Pradere, J.P., Hernandez, C., Gwak, G.Y., Caviglia, J.M., Mu, X., Loike, J.D., and Schwabe, R.F. (2015). The HMGB1/RAGE axis triggers neutrophil-mediated injury amplification following necrosis. J. Clin. Invest. *125*, 539–550.

Jensen, K.B., Driskell, R.R., and Watt, F.M. (2010). Assaying proliferation and differentiation capacity of stem cells using disaggregated adult mouse epidermis. Nat. Protoc. *5*, 898–911.

Jorch, S.K., and Kubes, P. (2017). An emerging role for neutrophil extracellular traps in noninfectious disease. Nat. Med. *23*, 279–287.

Kang, R., Zhang, Q., Zeh, H.J., 3rd, Lotze, M.T., and Tang, D. (2013). HMGB1 in cancer: good, bad, or both? Clin. Cancer Res. *19*, 4046–4057.

Khandpur, R., Carmona-Rivera, C., Vivekanandan-Giri, A., Gizinski, A., Yalavarthi, S., Knight, J.S., Friday, S., Li, S., Patel, R.M., Subramanian, V., et al. (2013). NETs are a source of citrullinated autoantigens and stimulate inflammatory responses in rheumatoid arthritis. Sci. Transl. Med. *5*, 178ra40.

Kim, Y.M., Park, E.J., Kim, J.H., Park, S.W., Kim, H.J., and Chang, K.C. (2016). Ethyl pyruvate inhibits the acetylation and release of HMGB1 via effects on SIRT1/STAT signaling in LPS-activated RAW264.7 cells and peritoneal macrophages. Int. Immunopharmacol. *41*, 98–105.

Kokkola, R., Li, J., Sundberg, E., Aveberger, A.C., Palmblad, K., Yang, H., Tracey, K.J., Andersson, U., and Harris, H.E. (2003). Successful treatment of collagen-induced arthritis in mice and rats by targeting extracellular high mobility group box chromosomal protein 1 activity. Arthritis Rheum. *48*, 2052–2058.

Konig, M.F., and Andrade, F. (2016). A Critical Reappraisal of Neutrophil Extracellular Traps and NETosis Mimics Based on Differential Requirements for Protein Citrullination. Front. Immunol. *7*, 461.

Li, P., Li, M., Lindberg, M.R., Kennett, M.J., Xiong, N., and Wang, Y. (2010). PAD4 is essential for antibacterial innate immunity mediated by neutrophil extracellular traps. J. Exp. Med. *207*, 1853–1862.

Menegazzo, L., Ciciliot, S., Poncina, N., Mazzucato, M., Persano, M., Bonora, B., Albiero, M., Vigili de Kreutzenberg, S., Avogaro, A., and Fadini, G.P. (2015). NETosis is induced by high glucose and associated with type 2 diabetes. Acta Diabetol. *52*, 497–503.

Moore, R.J., Owens, D.M., Stamp, G., Arnott, C., Burke, F., East, N., Holdsworth, H., Turner, L., Rollins, B., Pasparakis, M., et al. (1999). Mice deficient in tumor necrosis factor-alpha are resistant to skin carcinogenesis. Nat. Med. *5*, 828–831.

Papayannopoulos, V. (2018). Neutrophil extracellular traps in immunity and disease. Nat. Rev. Immunol. *18*, 134–147.

Park, J.S., Arcaroli, J., Yum, H.K., Yang, H., Wang, H., Yang, K.Y., Choe, K.H., Strassheim, D., Pitts, T.M., Tracey, K.J., and Abraham, E. (2003). Activation of gene expression in human neutrophils by high mobility group box 1 protein. Am. J. Physiol. Cell Physiol. *284*, C870–C879.

Park, J., Wysocki, R.W., Amoozgar, Z., Maiorino, L., Fein, M.R., Jorns, J., Schott, A.F., Kinugasa-Katayama, Y., Lee, Y., Won, N.H., et al. (2016). Cancer cells induce metastasis-supporting neutrophil extracellular DNA traps. Sci. Transl. Med. *8*, 361ra138.

Petrof, G., Abdul-Wahab, A., Proudfoot, L., Pramanik, R., Mellerio, J.E., and McGrath, J.A. (2013). Serum levels of high mobility group box 1 correlate with disease severity in recessive dystrophic epidermolysis bullosa. Exp. Dermatol. *22*, 433–435.

Polykratis, A., Hermance, N., Zelic, M., Roderick, J., Kim, C., Van, T.M., Lee, T.H., Chan, F.K.M., Pasparakis, M., and Kelliher, M.A. (2014). Cutting edge: RIPK1 Kinase inactive mice are viable and protected from TNF-induced necroptosis in vivo. J. Immunol. *193*, 1539–1543.

Scaffidi, P., Misteli, T., and Bianchi, M.E. (2002). Release of chromatin protein HMGB1 by necrotic cells triggers inflammation. Nature *418*, 191–195.

Straino, S., Di Carlo, A., Mangoni, A., De Mori, R., Guerra, L., Maurelli, R., Panacchia, L., Di Giacomo, F., Palumbo, R., Di Campli, C., et al. (2008). High-mobility group box 1 protein in human and murine skin: involvement in wound healing. J. Invest. Dermatol. *128*, 1545–1553.

Tadie, J.M., Bae, H.B., Jiang, S., Park, D.W., Bell, C.P., Yang, H., Pittet, J.F., Tracey, K., Thannickal, V.J., Abraham, E., and Zmijewski, J.W. (2013). HMGB1 promotes neutrophil extracellular trap formation through interactions with Toll-like receptor 4. Am. J. Physiol. Lung Cell. Mol. Physiol. *304*, L342–L349.

Taniguchi, N., Kawahara, K., Yone, K., Hashiguchi, T., Yamakuchi, M., Goto, M., Inoue, K., Yamada, S., Ijiri, K., Matsunaga, S., et al. (2003). High mobility group box chromosomal protein 1 plays a role in the pathogenesis of rheumatoid arthritis as a novel cytokine. Arthritis Rheum. *48*, 971–981.

Tarutani, M., Itami, S., Okabe, M., Ikawa, M., Tezuka, T., Yoshikawa, K., Kinoshita, T., and Takeda, J. (1997). Tissue-specific knockout of the mouse Pig-a gene reveals important roles for GPI-anchored proteins in skin development. Proc. Natl. Acad. Sci. USA *94*, 7400–7405.

Tirone, M., Tran, N.L., Ceriotti, C., Gorzanelli, A., Canepari, M., Bottinelli, R., Raucci, A., Di Maggio, S., Santiago, C., Mellado, M., et al. (2018). High mobility group box 1 orchestrates tissue regeneration via CXCR4. J. Exp. Med. *215*, 303–318.

Toussaint, M., Jackson, D.J., Swieboda, D., Guedán, A., Tsourouktsoglou, T.D., Ching, Y.M., Radermecker, C., Makrinioti, H., Aniscenko, J., Bartlett, N.W., et al. (2017). Host DNA released by NETosis promotes rhinovirus-induced type-2 allergic asthma exacerbation. Nat. Med. *23*, 681–691.

Wang, H., Bloom, O., Zhang, M., Vishnubhakat, J.M., Ombrellino, M., Che, J., Frazier, A., Yang, H., Ivanova, S., Borovikova, L., et al. (1999). HMG-1 as a late mediator of endotoxin lethality in mice. Science *285*, 248–251.

Wang, Y., Li, M., Stadler, S., Correll, S., Li, P., Wang, D., Hayama, R., Leonelli, L., Han, H., Grigoryev, S.A., et al. (2009). Histone hypercitrullination mediates chromatin decondensation and neutrophil extracellular trap formation. J. Cell Biol. *184*, 205–213.

Warnatsch, A., Ioannou, M., Wang, Q., and Papayannopoulos, V. (2015). Inflammation. Neutrophil extracellular traps license macrophages for cytokine production in atherosclerosis. Science *349*, 316–320.

West, K.L., Castellini, M.A., Duncan, M.K., and Bustin, M. (2004). Chromosomal proteins HMGN3a and HMGN3b regulate the expression of glycine transporter 1. Mol. Cell. Biol. *24*, 3747–3756.

Wong, S.L., Demers, M., Martinod, K., Gallant, M., Wang, Y., Goldfine, A.B., Kahn, C.R., and Wagner, D.D. (2015). Diabetes primes neutrophils to undergo NETosis, which impairs wound healing. Nat. Med. *21*, 815–819.

Yang, H., Hreggvidsdottir, H.S., Palmblad, K., Wang, H., Ochani, M., Li, J., Lu, B., Chavan, S., Rosas-Ballina, M., Al-Abed, Y., et al. (2010). A critical cysteine is required for HMGB1 binding to Toll-like receptor 4 and activation of macrophage cytokine release. Proc. Natl. Acad. Sci. USA *107*, 11942–11947.

Yuo, A., Kitagawa, S., Kasahara, T., Matsushima, K., Saito, M., and Takaku, F. (1991). Stimulation and priming of human neutrophils by interleukin-8: cooperation with tumor necrosis factor and colony-stimulating factors. Blood *78*, 2708–2714.

STAR★METHODS

KEY RESOURCES TABLE

REAGENT or RESOURCE	SOURCE	IDENTIFIER
Antibodies		
Histone-3 (citrulline R2+R8+R17)	abcam	Cat# ab5103; RRID: AB_ 304752
neutrophil elastase	Santa-Cruz	Cat# SC-9521; RRID: AB_2096537
HMGB1	abcam	Cat# ab79823; RRID: AB_1603373
TNF (for IHC)	R&D Systems	Cat# MAB610; RRID: AB_2203945
TNF (for blocking experiments)	Bioceros	MP6-XT22
TLR-4 blocking	Novimmune	5E3
Integrin alpha-6 (CD49f)	BD Biosciences	Cat# 555734; RRID: AB_2296273
Fc block (CD16/CD32)	BD Biosciences	Cat# 553141; RRID: AB_394656
CD45-PE conjugated	BD Biosciences	Cat# 553081; RRID: AB_394611
CD11b-BV421 conjugated	BD Biosciences	Cat# 562605; RRID: AB_11152949
Ly6G-APC conjugated	BD Biosciences	Cat# 560599; RRID: AB_1727560
CD64-BV711 conjugated	BD Biosciences	Cat# 740782; RRID: AB_2740445
Viability dye L/D eFluor780	eBiosciences	Cat# 65-0865-14
Chemicals, Peptides, and Recombinant Proteins		
RAGE antagonistic peptide	R&D Systems	Cat# 6259
TPA (phorbol 12-myristate 13-acetate	Sigma	Cat# P-8139
DMBA (7,12-dimethylbenzaanthracene	Sigma	Cat# D-3254
Ethyl pyruvate	Sigma	Cat# E47808
Streptozotocin	Sigma	Cat# S0130
DNase1	Roche	Cat#04536282001
Critical Commercial Assays		
HMGB1 ELISA	Tecan	Cat#ST51011
Deposited Data		
RNAseq data	This paper	GSE138918
Experimental Models: Cell Lines		
Normal human keratinocytes	Mulder lab	n/a
SCC keratinocytes	Mulder lab	n/a
Experimental Models: Organisms/Strains		
Mouse: HMGB1$^{fl/fl}$	Huebener et al., 2014	JAX#031274
Mouse: InvEE	Hobbs et al., 2004	n/a
Mouse: LysM Cre: B6.129P2-Lyz2tm1(cre)/lfo/J	The Jackson Laboratory	JAX#004781
Mouse: K5Cre	Tarutani et al., 1997	n/a
Mouse: RIPK1$^{D138N/D138N}$ kinase-inactive	Polykratis et al., 2014	n/a
Oligonucleotides		
Cxcl2 Fp: CAGACTCCAGCCACACTTCA	This paper	n/a
Cxcl-2 Rp: CACATCAAGCTCTGGATGTT	This paper	n/a
RANTES Fp: CACTTGCTGCTGGTG TAGAAA	This paper	n/a
RANTES Rp; CCCTCACCATCATCCTCACT	This paper	n/a
GAPDH Fp; AACATCAAATGG GGTGAGGCC	This paper	n/a
GAPDH Rp; GTTGTCATGGATGA CCTTGGC	This paper	n/a

LEAD CONTACT AND MATERIALS AVAILABILITY

Further information and requests for resources and reagents may be directed to Esther Hoste (Lead Contact; Esther.Hoste@irc.vib-ugent.be). Transfer of materials may require a material transfer agreement to be signed.

EXPERIMENTAL MODEL AND SUBJECT DETAILS

Mice

HMGB1 'floxed' (Huebener et al., 2014), InvEE (Hobbs et al., 2004), Keratin-5 (K5)-Cre (Tarutani et al., 1997), Lysozyme M (LysM)-Cre (Clausen et al., 1999) and RIPK1^{D138N} (Polykratis et al., 2014) mice have been previously described. InvEE mice were maintained on a mixed CBA x C57/Bl6 background and kept heterozygous for the MEK1 transgene. Transgene-negative HMGB1$^{fl/fl}$ littermates were used as controls. Both female and male mice of 7 to 18 weeks old were used and no mice died as a direct result of wounding or tumor formation and mice of the indicated genotype were assigned to groups at random. Mouse studies as well as immunostainings were performed in a blinded fashion.

Isolation and culture conditions of keratinocytes

Primary mouse keratinocytes were isolated from HMGB1$^{fl/fl}$ and Δ^{Ker} HMGB1 mouse back skin as described previously (Jensen et al., 2010) and cultured on feeders. Briefly, shaved back skin was isolated, sterilized and floated on trypsin overnight. Epidermis was separated from the dermis and cultured on confluent feeders. Human keratinocyte cell lines were cultured on feeders. Once keratinocyte cultures reached confluency, a medium switch to keratinocyte serum-free medium (KSFM) containing 30 μg ml-1 bovine pituitary extract was performed. Conditioned medium from these cultures was isolated after 48 hours.

Study approval

All animal procedures were conducted in accordance with European, national and institutional guidelines and protocols were subject to local ethical approval by Ghent university Ethical Board (license number: LA 1400091/LA 2400526). All human samples were collected after informed, written consent and in accordance with Helsinki guidelines. The study protocol was approved by the Universities of Monterrey and DEBRA Chile.

METHOD DETAILS

Wound healing assays and wound-induced tumor formation

Full-thickness wounds on the back skin of shaved mice were made by using an 8 mm punch biopsy needle (Stiefel Instruments) under analgesia and general anesthesia in 7 to 20 weeks-old aged- and sex-matched transgenic and control littermates. Wound and tumor sizes were measured every other day by two independent researchers, who were blinded to group allocations. Both female and male mice were included and statistical power was calculated by the resource equation. Animals were randomly assigned to treatment groups and no animals were excluded from experiments. In conditions where mice were treated, animals were intradermally injected with Box A (250 μg), ethylpyruvate (40 mg/kg), DNase-1 (1000 units), TNF blocking antibody (MP6-XT22 Mab; 100 μg/injection/mouse), RAGE antagonistic peptide (R&D Systems: 100 μg/injection), or TLR-4 blocking antibody (Novimmune, clone 5E3; 100 μg/injection) in 200 μL PBS, respectively, at time of wounding and at 12, 24 and 36 hours after wounding. Control mice were injected with equal volumes of PBS or the appropriate IgG control antibody.

Chemical carcinogenesis protocols

For two-stage carcinogenesis, mice of 7 weeks old were shaved and topically treated with 100 nmol DMBA (Sigma-Aldrich), followed by three times weekly applications of 6 nmol TPA (Sigma-Aldrich) in 200 μL of acetone for 15 weeks. Papillomas and SCCs were monitored once a week by two independent researchers, who were blinded to group allocations. For complete carcinogenesis, mice were topically treated with 5 μg DMBA in 200 μL of acetone twice a week for 20 weeks.

Induction of type 1 diabetes by streptozotocin injections

Diabetes induction was performed by multiple low-dose injections of streptozotocin (STZ; Sigma). 5 to 12-week old male mice were randomized into treatment groups and fasted for 8 hours overnight and injected intraperitoneal with vehicle or STZ (50 mg/kg per day, pH4, dissolved in 0.1 M sodium citrate buffer) for 5 consecutive days. Fed blood glucose levels were measured weekly starting 2 weeks after last injection. Mice with fed glucose levels above 300 mg/dl for 3 consecutive weeks were considered diabetic and used for further experiments.

Immunofluorescence

Paraffin sections were labeled with rabbit anti-histone-3 citrullinated Ab (H3^{citr}; 1:500; citrulline R2+R8+R17; Abcam ab5103; lot: 543646), goat anti-neutrophil elastase (NE; 1: 500; Santa Cruz SC-9521) or rabbit anti-HMGB1 antibody (1:500; Abcam ab79823 clone EPR 3507) for one hour. As secondary antibodies donkey-anti-goat 488 AlexaFluor (1:2000) and goat-anti-rabbit DyLight 586 (1:2000) were used in combination with Dapi.

Immunohistochemistry

Dewaxed paraffin sections were subjected to heat-mediated antigen retrieval (citrate buffer; pH = 6) and labeled with anti-TNF Ab (R&D Systems; 1:500). Slides were incubated with secondary antibody, followed by avidin-biotin complexes and peroxidase activity was detected with diaminobutyric acid (DAB) substrate (Vector Laboratories).

Western blotting

Unwounded, wounded or tumor-bearing skin was lysed in buffer containing 10 mM Tris-HCl at pH 7, 200 mM NaCl, 5 mM EDTA, 10% glycerol, 1% NP-40 and supplemented with complete EDTA-free Protease Inhibitor Cocktail Tablets (Roche Diagnostics) and Phospho-STOP Phosphatase Inhibitor Cocktail Tablets (Roche Diagnostics) and subsequently homogenized using Precellys beads. 20 μg of protein was separated on 15% SDS-PAGE and transferred to a nitrocellulose membrane. Immunoblotting was performed with rabbit anti-histone-3 citrullinated Ab (citrulline R2+R8+R17; GR314058-2; ab 5103; 1:1000; Abcam), rabbit anti-HMGB1 (1:500; Abcam), mouse anti-actin (1:10 000; BioConnect) antibodies and the appropriate HRP-coupled secondary antibodies (GE Healthcare). Detection was performed with the Western Lightning chemiluminescence reagent plus kit (PerkinElmer).

Flow cytometry

Immunophenotyping of wounded skin was performed on single-cell suspensions derived from mouse skin following trypsin digestion for 1 hour at 37°C and subsequent digestion with collagenase type 1 (1,25 mg/ml) (GIBCO), type 2 (0,5 mg/ml) (Sigma) and type 4 (0,5 mg/ml) (Sigma) for 30 to 45 min. Cells were stained with the following fluorochrome-linked antibodies: CD45-PE, CD11b-BV421, Ly6G-APC, CD64-BV711, anti-histone-3 citrullinated (citrulline R2+R8+R17; ab 5103; Abcam), L/D eFluor780 (eBiosciences) and Fc receptor-blocking antibody CD16/CD32 (clone 2.4G2, BD Biosciences). Prior to measuring, counting beads (Life Technologies) were added to the cells. Flow sorting of live mouse keratinocytes was performed after staining for integrin alpha-6 (BD BioScienes) on single-cell suspensions derived from epidermis isolated as previously described (Jensen et al., 2010). Measurements were performed on a BD Fortessa cytometer and analyzed using FlowJo software (Tree Star).

Recombinant mHMGB1 A-box expression and purification

pGEX-6P-2-mHMGB1 A-box plasmid was transformed in *E.coli* strain BL21(DE3). Exponentially growing cultures were induced with 0.5 mM isopropyl-β-D-thiogalactopyranoside and incubated at 20°C for 4h. Cell pellets were resuspended in buffer A [10 mM Na_2HPO_4 pH 7.4, 500 mM NaCl, 0.5 mM DTT, DNase 1 (1 mg/100 mL, Roche Diagnostics) and complete EDTA-free Protease Inhibitor Cocktail Tablets (Roche Diagnostics)], and lysed by sonication. Insoluble proteins were removed by centrifugation. The supernatant was incubated with DEAE resin (GE Healthcare) pre-equilibrated with buffer A. The DEAE flow-through fraction was applied to a glutathione Sepharose 4FF column (GE Healthcare) pre-equilibrated with buffer B (PBS pH 7.4). GST-tagged mHMGB1 A-box was eluted from the column with buffer C (50 mM Tris-HCl pH 8.5, 300 mM NaCl, 40 mM reduced glutathione). Elution fractions containing GST- mHMGB1 A-box were pooled and desalted against buffer D (50 mM Tris-HCl pH 7.0, 150 mM NaCl, 1 mM EDTA, 1 mM DTT). The GST- mHMGB1 A-box fusion protein was digested with the PreScission Protease (GE Healthcare) to clip off GST. The digested sample was run on a glutathione Sepharose 4B column (GE Healthcare) pre-equilibrated with buffer B for removal of the GST-tag and the PreScission Protease. Flow-through fractions containing mHMGB1 A-box, were pooled. After a buffer exchange step to buffer E (40 mM HEPES pH 7.4), the purified recombinant mHMGB1 A-box protein was applied to SP Sepharose FF (GE Healthcare) and eluted in buffer F (2x PBS pH 7.4). The elution fractions containing mHMGB1 A-box were pooled and diluted to 1x PBS pH 7.4. The purity of the fractions was checked by means of SDS-PAGE.

Primary keratinocyte cultures and scratch-wound assays

Primary keratinocytes obtained from Δ^{Ker} HMGB1 and control mice were obtained as previously described (Jensen et al., 2010). Scratching was performed on confluent keratinocyte cultures and wound closure was monitored by repetitive imaging.

RNA isolation and qPCR

RNA was isolated from tissues by column purification (QIAGEN RNeasy mini). Following reverse transcription, qPCR analysis was performed using primer-pairs against Cxcl-2 (Fp: CAGACTCCAGCCACACTTCA; Rp: CACATCAAGCTCTGGATGTT), RANTES (Fp: CACTTGCTGCTGGTGTAGAAA; Rp: CCCTCACCATCATCCTCACT) and normalized to GAPDH (Fp: AACATCAAATGGGG TGAGGCC; Rp: GTTGTCATGGATGACCTTGGC).

Cytokine measurements

HMGB1 levels in serum and conditioned medium were determined by ELISA according to the manufacturer's instructions (Tecan). Serum levels of TNF, IL-6 and IL-8 were determined by magnetic bead-based multiplex assay (eBioSciences).

RNA sequencing and bioinformatics

RNA (RIN > 8, as determined by Bioanalyzer 2100, Agilent) was isolated from live keratinocytes sorted from $HMGB1^{fl/fl}$ (n = 4) and Δ^{Ker} HMGB1 (n = 4) mice. Libraries were constructed using the Illumina TruSeq RNA Preparation Kit. RNA sequencing was performed at the VIB Nucleomics Core using HiSeq4000 SR50 (Illumina). The preprocessing of the RNA sequencing data was done by

Trimmomatic. The adapters were cut off, and reads were trimmed when the quality dropped below 20. Reads with a length < 35 were discarded. All samples passed quality control based on the results of FastQC. Reads were mapped to the mouse reference genome (mm10) via Tophat2 and counted via HTSeqCount. Samples were subsequently analyzed using R/Bioconductor, and the R package limma was used to normalize the data and to perform differential expression analysis. Benjamini-Hochberg was used to adjust the p values for multiple testing. For the analysis of DE genes, we applied limma-treat with a stringency level where the adjusted p value needs to be lower than 0.05 and the log2FC lower than −1 or higher than 1. For the heatmap we scaled the normalized log2 expression values per gene by calculating the mean expression per gene and then subtracting that mean value of each expression value.

Isolation of polymorphonuclear leukocytes

20 mL of heparinized blood was isolated from each healthy donor. 15 mL of PBS without calcium and magnesium (Thermo Fisher Scientific) was added and the suspension was applied on 15ml of Ficoll (Bio-Rad). Cells were centrifuged at 1400 rpm for 30 min at room temperature and suspension above the buffy coat removed. The white layer containing PMNs was collected and erythrocytes were removed by short cycles of hypotonic lysis with deionized water.

Live Cell Imaging

Human PMN cultures seeded in an 8 well chamber (iBidi) and supplemented with 2,5 μM Sytox Green (Thermo Fischer Scientific) and 1 μM Hoechst (Thermo Fischer Scientific) were incubated with conditioned medium from human keratinocyte cultures or stimulated with TNF (1 μg/ml) or ionomycin (1 μg/ml). Live cell imaging was performed on an Axio Observer.Z1 (Zeiss, Germany) equipped with a CSU-X1 spinning-disk head (Yokogawa Corporation of America) and stage top incubator (5%CO_2, 37°C). DIC and fluorescence Images were acquired with a plan Apo 20x/0.8 objective every 10 minutes for a period of 24 hours using an EMCCD Image MX2 camera (Hamamatsu). Sytox Green and Hoechst were excited with respectively a 405 and 488 nm diode laser. Image processing and movie editing was carried out in ImageJ (NIH) and data analysis was done with Volocity 6.3.0 (Perkin Elmer).

QUANTIFICATION AND STATISTICAL ANALYSIS

Statistical details of experiments can be found in the figure legends and Results sections. At least four replicates were generally used for each experimental condition for *in vitro* and *ex vivo* experiments. For *in vivo* experiments, at least 7 mice were used per group and experimental sample sizes were determined on the basis of prior power calculations. Additional experiments may be performed when larger variation in data was observed, and data were pooled for analysis.

DATA AND CODE AVAILABILITY

The accession number for the RNA-sequencing data reported in this paper is Gene Expression Omnibus (GEO): GSE138918.